PCCP

Stereodynamic control of cold rotationally inelastic CO + HD collisions

Journal:	*Physical Chemistry Chemical Physics*
Manuscript ID	CP-ART-06-2021-002755.R1
Article Type:	Paper
Date Submitted by the Author:	27-Jul-2021
Complete List of Authors:	Jambrina, Pablo; University of Salamanca, Química Física Croft, James; University of Otago; Dodd-Walls Centre for Photonic and Quantum Technologies, Naduvalath, Balakrishnan; UNLV, Chemistry Aoiz, F.; Universidad Complutense de Madrid,

Cite this: DOI: 00.0000/xxxxxxxxxx

Stereodynamic control of cold rotationally inelastic CO + HD collisions

Pablo G. Jambrina,[a,*] James F. E. Croft,[b,c] Naduvalath Balakrishnan,[d] F. Javier Aoiz[e,*]

Received Date
Accepted Date

DOI: 00.0000/xxxxxxxxxx

Quantum control of molecular collision dynamics is an exciting emerging area of cold collisions. Co-expansion of collision partners in a supersonic molecular beam combined with precise control of their quantum states and alignment/orientation using Stark-induced Adiabatic Raman Passage allows exquisite stereodynamic control of the collision outcome. This approach has recently been demonstrated for rotational quenching of HD in collisions with H_2, D_2, and He and D_2 by He. Here we illustrate this approach for HD($v = 0$, $j = 2$)+CO($v = 0$, $j = 0$)→HD($v' = 0$, j')+CO($v' = 0$, j') collisions through full-dimensional quantum scattering calculations at collision energies near 1 K. It is shown that the collision dynamics at energies between 0.01–1 K are controlled by an interplay of $L = 1$ and $L = 2$ partial wave resonances depending on the final rotational levels of the two molecules. Polarized cross sections resolved into magnetic sub-levels of the initial and final rotational quantum numbers of the two molecules also reveal a significant stereodynamic effect in the cold energy regime. Overall, the stereodynamic effect is controlled by both geometric and dynamical factors, with parity conservation playing an important role in modulating these contributions depending on the particular final state.

1 Introduction

The extraordinary progress achieved in the last couple of decades in creating dense samples of cold and ultracold molecules has transformed our ability to control and interrogate the outcome of molecular collisions [1–7]. This progress has led to new applications of cold and ultracold molecules in precision molecular spectroscopy, quantum sensing, quantum information and computation, and quantum control of chemical reaction dynamics [8–11]. Ultracold molecules in their absolute rovibrational and motional ground states trapped in optical tweezers allow the realization of quantum engineering of molecular assembly for many-body dynamics [12,13], new quantum matter with exotic properties and molecular qubits for quantum computation and simulation [4,5,14].

Ultracold molecules offer unique opportunities to explore molecular collisions in the deep quantum regime. One such elementary molecular processes is a rotation-translation energy exchange in which a rotationally excited molecule undergoes relaxation (quenching) in collisions with an atom and the energy released is transferred to the relative translation of the collision partners. Such processes have been extensively studied in the literature for many neutral and ionic molecular systems, including the simplest molecule H_2 [15,16]. Collisions of H_2 and HD with He are important for modeling gas densities in astrophysical environments where non-equilibrium populations prevail [16,17]. At thermal energies, many partial waves contribute and the collision outcome is generally less sensitive to fine details of the interaction potential. However, at the lowest temperatures of interest in the interstellar medium (∼4 K), only a few partial waves contribute for light systems such as He+H_2, He+HD, and H_2+H_2. In this regime, collision outcomes are severely influenced by small changes in the interaction potential and isolated resonances due to tunneling through angular momentum barriers.

Currently there is much interest in studying inelastic and reactive molecular collisions near 1 K as well as in the mK (cold) and μK (ultracold) regimes [18–32]. Quantum effects are amplified in these regimes and quantum control of molecular collisions using external electric and magnetic fields becomes feasible [1–7]. While such control is most promising in the ultracold regime where only a single partial wave contributes, collision energies near 1 K are also of interest as collision outcomes are dominated by a few partial waves. The energy regime between 1 mK–1 K has been the focus of many experiments involving co-

[a] Departamento de Química Física. University of Salamanca, Salamanca 37008, Spain. e-mail: pjambrina@usal.es
[b] Department of Physics, University of Otago, Dunedin 9054, New Zealand. e-mail: j.croft@otago.ac.nz
[c] Dodd-Walls Centre for Photonic and Quantum Technologies, Dunedin 9054, New Zealand.
[d] Department of Chemistry and Biochemistry, University of Nevada, Las Vegas, NV 89154, USA. e-mail: naduvala@unlv.nevada.edu
[e] Departamento de Química Física. Universidad Complutense. Madrid 28040, Spain. e-mail:aoiz@quim.ucm.es

expansion[33,34] and merged beam techniques[35–37] in which sensitive measurements of isolated resonances have been reported for Penning ionization of molecules such as H_2 and HD by rare gas atoms in excited electronic states. The regime near 1 K has also been the focus of a series of experiments by Perreault et al. in which rotational quenching of HD by H_2, D_2 and He has been reported[18–22]. The experiment involves co-expansion of the molecular species in a supersonic beam combined with selection of the initial orientation of the molecular rotational angular momentum through Stark-induced adiabatic Raman Passage (SARP). The SARP method allows stereodynamic control of the collision process by selecting a given projection (m_j) of the molecular rotational angular momentum j on the relative collision velocity vector or preparing a molecular state in a coherent superposition of m_j states. For collision partners such as H_2 and HD or HD/D_2 and He, the co-expansion can achieve a narrow distribution of relative molecular velocities corresponding to collision energies in the vicinity of 1 Kelvin, drastically limiting the number of angular momentum partial waves. Yet, experimental results do not provide explicit energy resolution and theoretical studies are needed to identify specific partial wave resonances that contribute to distinct features in the experimental angular distribution or collision mechanism[38,39]. Computational studies have been critical in yielding mechanistic insights into recent experiments on HD($v=1$, $j=2\rightarrow v'=0$, $j'=0$) quenching by H_2 and He[23–25,29].

Calculations have also demonstrated that stereodynamic control extends to cases where there are overlapping resonances from multiple partial waves[28,40] making it possible to disentangle the resonance pattern. Moreover, calculations have also identified strong stereodynamic preference in the $m_j - m_{j'}$ resolved integral and differential cross sections in the ultracold s-wave regime for rotational quenching of HD by He[29].

So far, the experiments on state prepared HD with He and H_2/D_2 involved no change in rotational levels of the collision partners (H_2/D_2) limiting the number of partial waves in the outgoing channel and complexity of the collision dynamics. However, it is not clear whether stereodynamic control of the collision outcome is still possible when both collision partners change their rotational states. Here, we consider HD($v=0$, $j=2$)+CO($v=0$, $j=0$)$\rightarrow$HD($v'=0$, j')+CO($v'=0$, j') collisions in which rotational levels of both molecules are altered during the collision leading to more intricate collision dynamics. Moreover, and unlike HD+H_2/He systems, the interaction potential for CO+H_2 is deeper and more anisotropic, offering a more stringent case for stereodynamical control in the cold regime. However, the difference of mass between the two partners will likely limit the access to sufficiently low collision energies due to the difference of terminal velocities between CO and HD in co-expansions as those used in SARP experiments. A judicious choice of initial velocity for either species might mitigate this problem.

Collisions of molecular hydrogen with CO are important processes in astrophysical environments and has attracted considerable experimental and theoretical attention in recent years[41–51]. Its importance stems from the fact that CO is the second most abundant molecule in the interstellar medium after H_2 and is often used as a tracer of H_2 in dense interstellar clouds due to its dipole moment. Several theoretical studies have reported temperature dependent rate coefficients for rotational and rovibrational transitions in CO due to H_2 collisions of interest in astrophysical media[43,46–51]. Highly accurate measurements of CO rotational excitation cross sections by H_2 have also been reported allowing direct comparisons with theoretical predictions[46–48,50,51]. The most recent full-dimensional potential energy surface (PES) for the H_2-CO complex[45,51] has yielded rotational excitation cross sections in close agreement with experiment[48,50] as well as high accuracy spectroscopic data[42,44]. While CO+H_2 collisions have been extensively studied, CO+HD collisions have received limited attention, and we are not aware of any prior theoretical studies. The experimental measurements have reported anomalously large rate coefficients for vibrational relaxation of CO($v=1$) by HD compared to H_2 and D_2 collision partners[52–54]. Here we focus on rotational relaxation of HD($v=0$, $j=2$) by CO($v=0$, $j=0$) in which the HD molecule is prepared in various stereodynamic alignment/orientations.

2 Theoretical Approach

2.1 Scattering calculations

Scattering calculations were performed in full-dimensionality using a modified version of the TwoBC code[55], which implements a time-independent close-coupling formalism yielding the scattering S matrix[56]. This approach has has been outlined in detail elsewhere[57–59]. While excited vibrational levels are included in the basis set we only examine transitions between rotations levels in the ground vibrational manifold and as such, for convenience, we label each asymptotic channel by the combined molecular state $\alpha = j_1 j_2$, where j is the rotational quantum number. In this work the subscript 1 refers to HD and 2 to CO. The integral cross section for state-to-state rotationally inelastic scattering is given by,

$$\sigma_{\alpha\rightarrow\alpha'} = \frac{\pi}{(2j_1+1)(2j_2+1)k_\alpha^2} \sum_J \sum_{j_{12},j'_{12}} \sum_{L,L'} (2J+1)|T^J_{\alpha L j_{12},\alpha' L' j'_{12}}|^2, \quad (1)$$

where $k_\alpha^2 = 2\mu E_{\rm coll}/\hbar^2$ is the square of the initial relative wave vector, $E_{\rm coll}$ is the collision energy, μ is the reduced mass, $T^J = 1 - S^J$, $\vec{j}_{12} = \vec{j}_1 + \vec{j}_2$, L is the orbital angular momentum quantum number, and J the total angular momentum quantum number where $\vec{J} = \vec{L} + \vec{j}_{12}$.

For the PES we used the recent high-accuracy 6D CO+H_2 potential reported by Faure et al.[60,61]. This potential was chosen as it reproduces the proper physical inverse-power dependence with the intermolecular distance, R, at long range which is crucial for low energy collisions. To account for the difference in centre of mass between H_2 and HD a coordinate rotation was implemented as described in Ref. 62. Jacobi vectors were employed to describe the relative positions of the atoms with $\vec{r}_1(r_1,\hat{r}_1)$ denoting the vector connecting H with D, $\vec{r}_2(r_2,\hat{r}_2)$ denoting the vector connecting C with O, and $\vec{R}(R,\hat{R})$ denoting the vector joining the centers of mass of the two molecules. The angular dependence of the potential was expanded as

$$U(\vec{r}_1,\vec{r}_2,\vec{R}) = \sum_\lambda A_\lambda(r_1,r_2,R) Y_\lambda(\hat{r}_1,\hat{r}_2,\hat{R}), \quad (2)$$

with

$$Y_\lambda(\hat{r}_1,\hat{r}_2,\hat{R}) = \sum_m \langle \lambda_1 m_1 \lambda_2 m_2 | \lambda_{12} m_{12}\rangle Y_{\lambda_1 m_1}(\hat{r}_1) Y_{\lambda_2 m_2}(\hat{r}_2) Y^*_{\lambda_{12} m_{12}}(\hat{R}), \quad (3)$$

where $\lambda \equiv \lambda_1\lambda_2\lambda_{12}$ and $m \equiv m_1 m_2 m_{12}$. For the scattering calculations λ_1 was restricted to 0–4 while λ_2 was restricted to 0–8.

The coupled channel equations were propagated from 2 to $92\,a_0$ with a radial step size of $1.25\times10^{-1}\,a_0$ using a log-derivative method[63]. The number of points in the radial coordinate for each dimer for the discrete variable representation was 18; the number of points in the angular coordinate θ between $\vec{R}$ and $\vec{r}$ for each dimer for the Chebyshev quadrature was 12; the number of points in the dihedral angle between θ_1 and θ_2 for the Gauss-Hermite quadrature was 8. The quadratures are the same as used by Yang et al. to study H_2 + CO collisions[47]. The basis set for the CO dimer included vibrational levels 0 and 1 with rotational levels up to 8 and 2 respectively, while for HD rotational levels up to 4 were included. Scattering calculations were performed for each parity for $J \leq 12$.

To ensure convergence with respect to the basis set and radial propagations, calculations were repeated for $J \leq 5$ using an expanded basis and a larger radial propagation (see Supplementary material for further calculations). As it is shown in Fig. S1, no appreciable difference is observed between the two set of calculations, and the low energy behavior is correctly reproduced.

2.2 Stereodynamics

To compute the differential cross sections (DCS) we need first to compute the scattering amplitude ($f_{m_1,m_2\to m_1',m_2'}$). From a given $\alpha\to\alpha'$ transition, the scattering amplitude in the helicity representation is given by[64]:

$$f_{m_1,m_2\to m_1',m_2'} = \frac{1}{2k_\alpha}\sum_J (2J+1) \sum_{j_{12},j_{12}',L,L'} i^{L-L'+1} d^J_{m_{12},m'12}(\theta)$$
$$\times T^J_{\alpha L j_{12}\alpha' L' j_{12}'} \langle j_{12}' m_{12}', J-m_{12}'|L'0\rangle \langle j_{12} m_{12}, J-m_{12}|L0\rangle \quad (4)$$
$$\times \langle j_1' m_1', j_2' m_2'|j_{12}' m_{12}'\rangle \langle j_1 m_1, j_2 m_2|j_{12} m_{12}\rangle$$

where $m_{12} = m_1 + m_2$, $m_{12}' = m_1' + m_2'$ (otherwise the last two Clebsch Gordan coefficients are zero), and where α and α' have been omitted for the sake of clarity. In Eq. 4, θ is the scattering angle, $d^J_{m_{12},m_{12}'}(\theta)$ is Wigner's reduced rotation matrix, and $\langle\ldots|\ldots\rangle$ is a Clebsch-Gordan coefficient. The DCS can be calculated as:

$$\mathrm{DCS} \equiv \frac{d\sigma}{d\omega} = \frac{1}{(2j_1+1)(2j_2+1)} \sum_{m_1,m_2}\sum_{m_1',m_2'} f^*_{m_1,m_2\to m_1',m_2'} f_{m_1,m_2\to m_1',m_2'} \quad (5)$$

Similarly, three-vector correlations can be calculated in terms of the polarization dependent differential cross sections (PDDCS)[65]. Specifically, for the $\boldsymbol{k}$-$\boldsymbol{j}_1$-$\boldsymbol{k}'$ correlations, where $\boldsymbol{k}$ and $\boldsymbol{k}'$ are the initial and final relative velocities, the corresponding reactant's PDDCS (or j-PDDCSs), $U^{(k)}_q(\theta)$, can be calculated as follows[65]:

$$U^{(k)}_q(\theta) = \frac{1}{(2j_1+1)(2j_2+1)} \sum_{m_1}\sum_{m_2}\sum_{m_1',m_2'} f^*_{m_1,m_2\to m_1',m_2'} f_{m_1+q,m_2\to m_1',m_2'}$$
$$\times \langle j_1 m_1, kq | j_1 m_1 + q\rangle \quad (6)$$

where k and q are the rank and the component of the PDDCSs, and it is assumed that reactant 1 (HD) is polarized, while reactant 2 (CO) is unpolarized. These PDDCSs are those that are needed to simulate a SARP experiment where one of the reactants is polarized.

As described in Ref. 65, if one of the reactant partners is prepared in a directed state, $|j\ m=0\rangle$, its internuclear axis can be aligned along the laboratory quantization axis, which is usually the light polarization vector[66]. It is possible then to change the direction of the quantization (laboratory-fixed) axis with respect to the scattering frame, defined by $\boldsymbol{k}$ and $\boldsymbol{k}'$. The various directions of the polarization vector lead to different relative geometries of the reactants. In particular, the internuclear axis distribution for a given preparation is given by[65,67]

$$P(\theta_r,\phi_r) = \frac{1}{4\pi}\sum_k \sum_{q=-k}^{k} (2k+1)\left[\mathscr{A}^{(k)}_0 C_{kq}(\beta,\alpha)\right] C^*_{kq}(\theta_r,\phi_r), \quad (7)$$

where β and α are the polar and azimuthal angles that define the direction of the laboratory quantization axis with respect to the scattering frame, θ_r and ϕ_r define the direction of the relevant internuclear axis in the scattering frame. $C_{kq}(\beta,\alpha)$ (and $C_{kq}(\theta_r,\phi_r)$) are the modified spherical harmonics, and $\mathscr{A}^{(k)}_0$ are the polarization parameters that define the preparation in the laboratory frame.

In this scenario, the DCS for a given preparation of $\boldsymbol{j_1}$ is:

$$\left[\frac{\mathrm{d}\sigma}{\mathrm{d}\omega}\right]^\beta_\alpha = \sum_{k=0}^{2j_1}\sum_{q=-k}^{k} (2k+1)\mathscr{A}^{(k)}_0 U^{(k)}_q(\theta) C^*_{kq}(\beta,\alpha). \quad (8)$$

To obtain the integral cross section for the different experimentally achievable preparations, it is necessary to integrate $\left[\frac{\mathrm{d}\sigma}{\mathrm{d}\omega}\right]^\beta_\alpha$ over both θ and the azimuthal angle (for details see the appendix). Accordingly, the observable cross section depends only on β and will be denoted as σ^β.

As shown in the appendix, if the initial rotational state for reactant 1 in the laboratory frame is the pure $|j\,m=0\rangle$ state, hence the polarization parameters are given $\mathscr{A}^{(k)}_0 = \langle j0\, j0|k0\rangle$ and it is possible to express the (β,α) DCS directly in terms the scattering amplitudes:

$$\left[\frac{\mathrm{d}\sigma}{\mathrm{d}\omega}\right]^\beta_\alpha = \frac{1}{2j_2+1}\sum_{m_1'm_2'}\sum_{m_2}\left|\sum_{m_1} C_{j_1m_1}(\beta,\alpha) f_{m_1,m_2\to m_1',m_2'}\right|^2 \quad (9)$$

3 Results and Discussion

We will start this section showing the excitation function (cross section as a function of the collision energy) for the different final rovibrational states that can be produced in the collisions between HD(v=0,j=2) and CO(v=0,j=0) at cold energies, be-

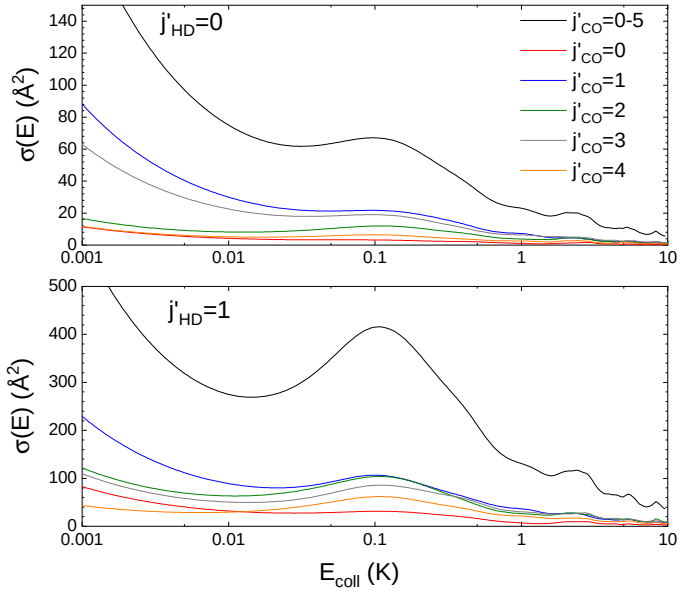

Fig. 1 Cross section as a function of the collision energy for HD(j_{HD}=2) + CO(j_{CO}=0) → HD(j'_{HD}=0,1) + CO(j'_{CO}=0–5) collisions. Results for j'_{HD}=0 are shown in the top panel and those for j'_{HD}=1 are shown in the bottom panel.

tween 1 mK and 10 K. Due to the large difference in the rotational constants of HD and CO (B_e=64.2 K and 2.8 K for HD and CO, respectively) only j'_{HD}=0-1 are energetically accessible for HD but many different CO rotational states can be populated in this energy regime. Throughout this manuscript, we will divide the final states according to the value of j'_{HD}. The first endoergic channel corresponding to (j'_{HD}=2, j'_{CO}=1) opens above 1 K, and has been omitted in our discussions.

Results displayed in Fig. 1 show that collisions leading to j'_{HD}=1 (Δj_{HD} =–1) have larger cross sections than those leading to j'_{HD}=0 (Δj_{HD} = –2). For a given j'_{HD}, collisions leading to j'_{CO}=1 are predominant, especially for $E_{coll} < 10$ mK, but that difference drops as the energy rises. This indicates that HD rotational energy is not efficiently transferred to CO. The most relevant feature of the excitation function is the presence of a resonance at around 0.1 K. The resonance peak is especially noteworthy for j'_{HD}=1, but it is present for almost every final state. Further analysis (see Fig. S2 and S3 in the supplementary material) demonstrated that this is a shape resonance mostly associated to L=2. The contribution of L=1 seems to be due to an "above-the-barrier" resonance.

To understand the origin of the resonance, and to determine the extent of control that can be achieved, we will focus on 4 different final states: (j'_{HD}=0, j'_{CO}=0) for which the effect of the resonance, if any, is almost negligible, and (j'_{HD}=1, j'_{CO}=1), (j'_{HD}=1, j'_{CO}=2), (j'_{HD}=1, j'_{CO}=3), the three states that are preferentially formed around the energy of the resonance. In the top panels of Fig. 2 we show the cross sections for these four states, and also the contribution of L=0–3 to the cross section. As expected, at low energies only L=0 contributes to the cross section, but with increasing collision energies contributions from other L become important. Around 0.1 K, the energy of the resonance peak, L=1 is the partial wave with the largest cross section, even for (j'_{HD}=0, j'_{CO}=0). Interestingly, the contribution of L=2 is rather different: for (j'_{HD}=1, j'_{CO}=1, 3) the contribution from L=2 to the resonance is about 50% that for L=1; however, for (j'_{HD}=1, j'_{CO}=2), (j'_{HD}=0, j'_{CO}=0) its relevance is significantly smaller. We can anticipate that the analogies between (j'_{HD}=1, j'_{CO}=1,3) will also manifest when we analyze both $\sigma^{J,L}$ and their behavior upon alignment of $\boldsymbol{j}_{HD}$.

In the two lower panels of Fig. 2, we show the partial cross sections for a given total and orbital angular momentum values. The results for L=1 and L=2 are displayed in the middle and bottom panels, respectively. The sum over all J, i.e. $\sigma(E;L)$, are shown as dashed lines. Parity ($P = (-1)^{j_{HD}+j_{CO}+L}$) conservation implies that not all (L,J) combinations are possible for (j'_{HD}=0, j'_{CO}=0) product channel. In this particular case, $L'=J$, hence parity is $(-1)^J$. Accordingly, only (L=even, J=even) and (L=odd, J=odd) combinations are possible, but combinations such as (L=1, J=2) are forbidden. For this state and L=1, J=1 and J=3 show similar cross sections at energies below the resonance, but J=3 prevails around the resonance. For the other three final states, the contribution from (L=1, J=1) is very minor, while those from (L=1, J=2) and (L=1, J=3) are similar. It is worth mentioning that while for (j'_{HD}=1, j'_{CO}=2), $\sigma(E;J=2,L=1)$ is larger, for j'_{CO}=1,3 $\sigma(E;J=2,L=3)$ prevails.

For L=2 differences between the four studied final states are substantial. For (j'_{HD}=0, j'_{CO}=0) parity conservation forbids the (J=1,3) channels, and the dominant term is (L=2, J=4). For j'_{HD}=1 states, the relative cross section of (L=2, J=4) is similar, and these peaks coexist with those observed for J=1,3. For j'_{HD}=1, the peak associated with $\sigma^{L=2}$ exhibits a double maximum, the first associated with J=1, and 4, and the second with J=2, and 3. The position of these peaks does not depend on the final state, although the relative contribution of L=2 to the resonance plays an important role (see above). For the inelastic collisions between H + HF Jambrina et al.[28] also observed different maxima for a given L, each of them associated with a different value of J. However, in the present case, the peak associated with a given J occurs at the same energy and their position does not depend on the final state.

It is also worth emphasizing that the relevant intensity of the partial cross sections for (L=2, J=1,3) depends on the final state. For (j'_{HD}=1, j'_{CO}=1,3) the J=1 peak is higher than that of J=3, especially for j'_{CO}=1. On the contrary, for (j'_{HD}=1, j'_{CO}=2) the J=3 peak is more intense than J=1 with a simultaneous increase in the intensity of the J=2 peak. As a result, the second maxima associated with L=2 is slightly higher than the first one, unlike what was observed for j'_{CO}=1,3. Again, the overall behavior of the j'_{CO}=1,3 partial cross sections is different from that of j'_{CO}=2.

To see if the intensity of the resonance peaks can be tuned by selecting the direction of the HD rotational angular momentum (hence of the internuclear axis) prior to the collision, we calculated the excitation function for different values of β, the angle between the polarization vector of the SARP laser and the initial relative velocity vector (see Fig. 3). With β=0° collisions will be preferentially head-on, while β=90° implies a side-on geometry. In fact, β=0° is equivalent to selecting $m_l = m_{HD}$=0. Between

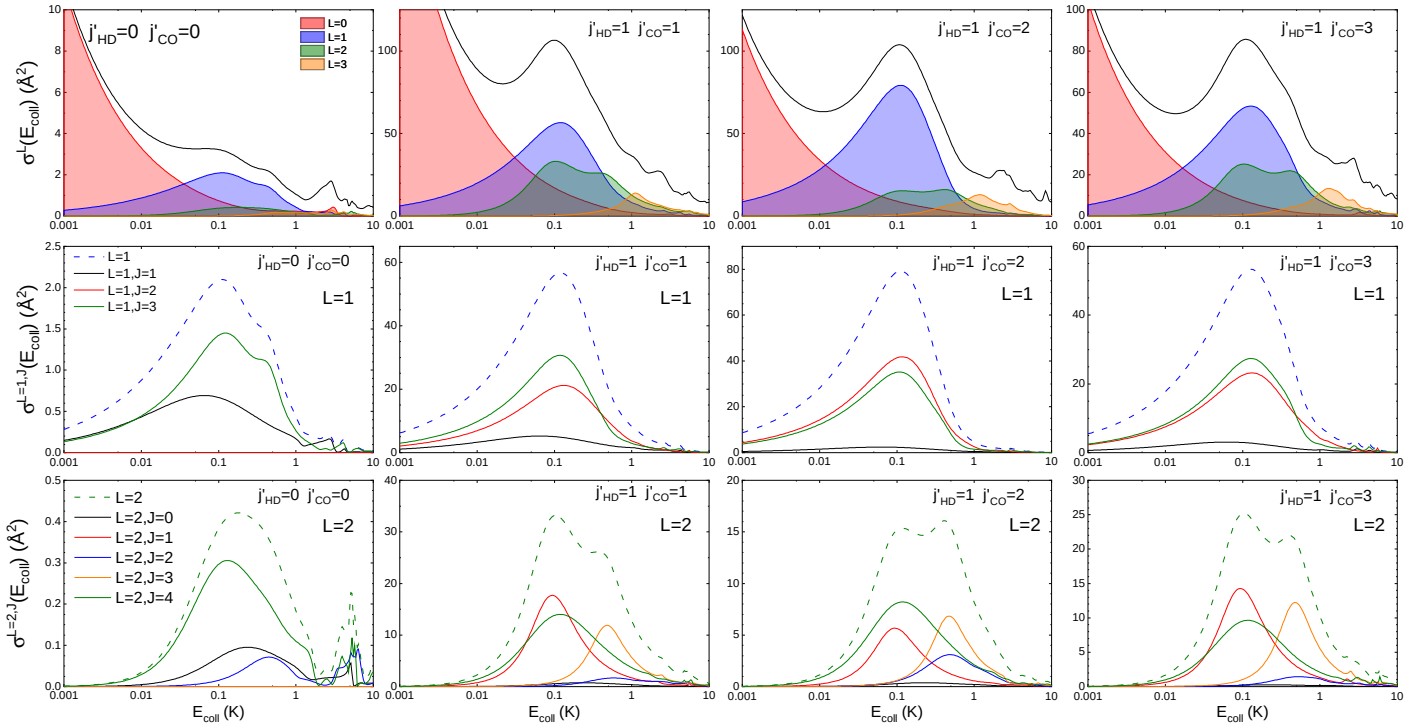

Fig. 2 Total and partial cross sections as a function of the collision energy for HD(j_{HD}=2) + CO(j_{CO}=0) $\rightarrow$ HD(j'_{HD}) + CO(j'_{CO}) collisions and four specific final states (see text for further details). The contribution of each L value is shown in the top panel and $\sigma(E_{coll};J,L)$ are shown in the middle (L=1) and bottom (L=2) panels. For symmetry reasons the number of possible (J, L) combinations depend on the final state considered.

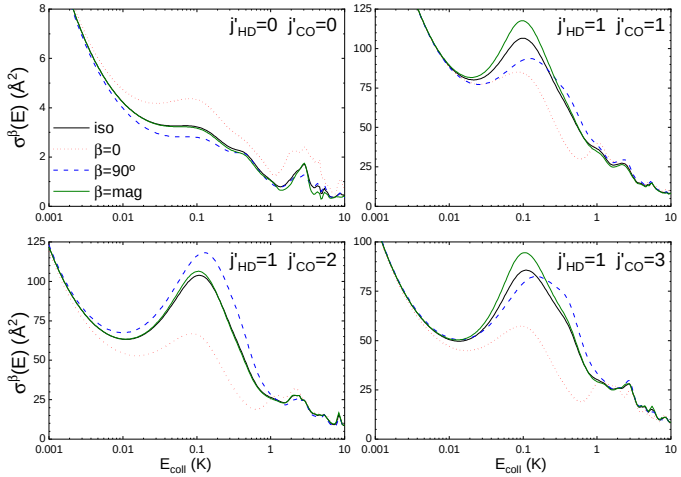

Fig. 3 Cross section as a function of the collision energy for HD(j_{HD}=2) + CO(j_{CO}=0) $\rightarrow$ HD(j'_{HD}) + CO(j'_{CO}) collisions for four specific final states and three different preparations of the HD intermolecular axis, β =0° (dotted red line), β =90° (dashed blue line), and the magic angle (solid olive line). The isotropic preparation (in the absence of external alignment) is shown in black

these two geometries, we will also calculate the excitation functions for "the magic angle" (β = mag), the angle for which the second Legendre polynomial is zero, that is, $\beta = \arccos(\sqrt{3}/3) \approx 54.74°$, and hence contribution of k=2, q=0 term in Eq. (8) vanishes).

The alignment-dependent excitation functions display three different patterns depending on the final state considered, as shown in Fig. 3. For (j'_{HD}=0, j'_{CO}=0), for which the effect of the resonance is very minor, the cross section is clearly enhanced for β=0° (head-on) collisions, in particular around the 0.1 K resonance, as well as above 1 K. It should be emphasized that as $E_{coll} \rightarrow 0$, the integral cross section becomes insensitive to changes in the relative alignment of the reactants.[68] In fact, if we only had L=0 (s-wave) encounters, there would not be any stereodynamical preference regardless of the initial and final state considered. Side-on (β=90°) collisions lead to slightly smaller cross sections, but the effect is not as noteworthy as for head-on encounters. If β = mag is selected, the cross section is nearly the same as if HD were not aligned (isotropic distribution).

The situation is different for j'_{HD}=1 states, for which the resonance has a salient effect. For these states, the stereodynamical control is strongly influenced by the resonance, and at energies above and below the resonance the relative alignment of HD has a negligible effect on the cross sections. Moreover, regardless of the final state, the cross section around the resonance drops for β=0° collisions, reaching its minimum value at around 0.6 K, beyond which it rises to the isotropic value. Again, there is a clear difference between j'_{CO}=1,3 and j'_{CO}=2. For (j'_{HD}=1, j'_{CO}=2), the cross section at the resonance is enhanced by the β=90° prepa-

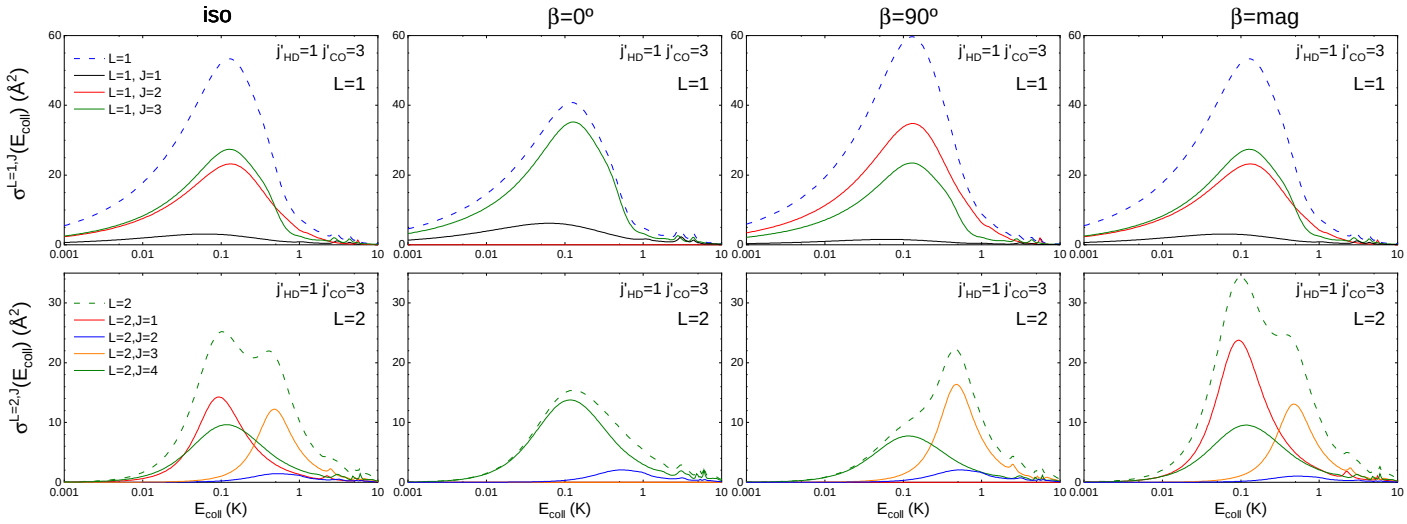

Fig. 4 $\sigma(E;J,L)$ partial cross sections as a function of the collision energy for HD(j_{HD}=2) + CO(j_{CO}=0) → HD(j'_{HD}=1) + CO(j'_{CO}=3) collisions for different preparations of the HD intermolecular axis. Results for L=1 are shown in the top panels and those for L=2 are shown in the bottom panels. Results for the isotropic distribution are identical to those depicted in Fig. 2 and are only shown here for the sake of comparison.

ration, while β = mag has only a very minor effect. However, for j'_{CO}=1,3, it is β = mag that leads to a significant enhancement of the cross section. $\sigma^{\beta=90^\circ}$, in turn, is somewhat smaller at the resonance peak and is shifted towards slightly higher collision energies.

To understand the origin of the different stereodynamical preferences, we show in Fig. 4 the $\sigma^{J,L}$ for the different HD alignments discussed above. In this case, we will focus on one particular final state, (j'_{HD}=1, j'_{CO}=3). β=0° leads to a smaller L=1 cross section. This is due to the absence of (L=1,J=2) term which is not compatible with β=0° (due to parity conservation). For L=2, β=0° leads to a modest increase of the cross section associated with J=2 and J=4, but it makes the terms associated with J odd vanish (again imposed by conservation of the parity). Altogether, it explains the decrease of the reactivity associated with β=0° for j'_{HD}=1 states. It also explains why β=0° leads to an increase of the partial cross section for (j'_{HD}=0, j'_{CO}=0). Conservation of parity requires that for (j'_{HD}=0, j'_{CO}=0) the S-matrix element associated with (L=odd, J=even) or (L=even, J=odd) must be zero, regardless of the collision partner's polarization. These are the elements that are zero for β=0° (since they do not contain m_1=0), so the only effect of this preparation is to enhance the contribution of the elements that are not zero by parity conservation, hence leading to an increase of the cross section for (j'_{HD}=0, j'_{CO}=0).

Back to (j'_{HD}=1, j'_{CO}=3), β=90° enhances the influence of (L=1, J=2) but decreases that of (L=1, J=1). The effect on L=2 is more important, as β=90° is not compatible with (L=2, J=1). Consequently, states for which the latter term was important show smaller cross sections for β=90°. Besides, the enhancement of the (L=2, J=3) element displaces the resonance peak to slightly higher energies. The reason behind the disappearance of (L=2, J=1) for β=90° can be found in Eq. (4). For j_1=2, L=2, and J=1, the second Clebsch-Gordan in Eq. 4 is zero unless m_{12}=1. And for m_{12}=1 and β=90° the cross-section is necessarily zero (see Eq. 24 in the appendix).

Finally, β=mag is compatible with all possible combinations of (J, L) and the term that is affected the most by this preparation is (L=2, J=1), whose cross section is significantly larger. As a result, cross sections for those final states for which (L=2, J=1) is important are enhanced by a β = mag preparation.

The main theme that emerges from these discussions is as follows. An anisotropic preparation of the reactants leads to the modification of the intensity of each J–L combination. However, how the stereodynamic preparation changes these terms depends on geometric factors and not on the final state, or any dynamical aspects. Nevertheless, the relative weight of every J–L contributions in the isotropic distribution has a dynamical origin. In particular, dynamical quantum effects such as resonances are responsible of sudden and important changes in the modulus of particular S-matrix elements. In the present case, the effect of the resonance is very sensitive to the final state considered, leading to different stereodynamical preferences. In other words, by measuring the cross section for different experimental preparations, it could be possible to disentangle the importance of the different J–L partial waves.

So far, we have only focused on how the different alignments affect the integral cross section. To see how they affect the DCS, in Fig. 5 we show the DCS and the scattering angle-recoil velocity polar maps at 0.1 K that could be experimentally measured detecting the HD rovibrational state. As mentioned above, the energy difference between two adjacent CO rotational states is considerably smaller than that between consecutive HD rotational levels. Therefore in the polar maps we observe two rings: one external (higher recoil velocities) associated with j'_{HD}=0 and an internal ring (lower recoil velocities) associated with j'_{HD}=1. Since the cross section for j'_{HD}=1 is almost one order of magnitude larger than that for j'_{HD}=0, the intensity of the internal ring is much higher. Along with the DCS and the polar maps, in the two upper panels of Fig. 5 we show the alignment-dependent excita-

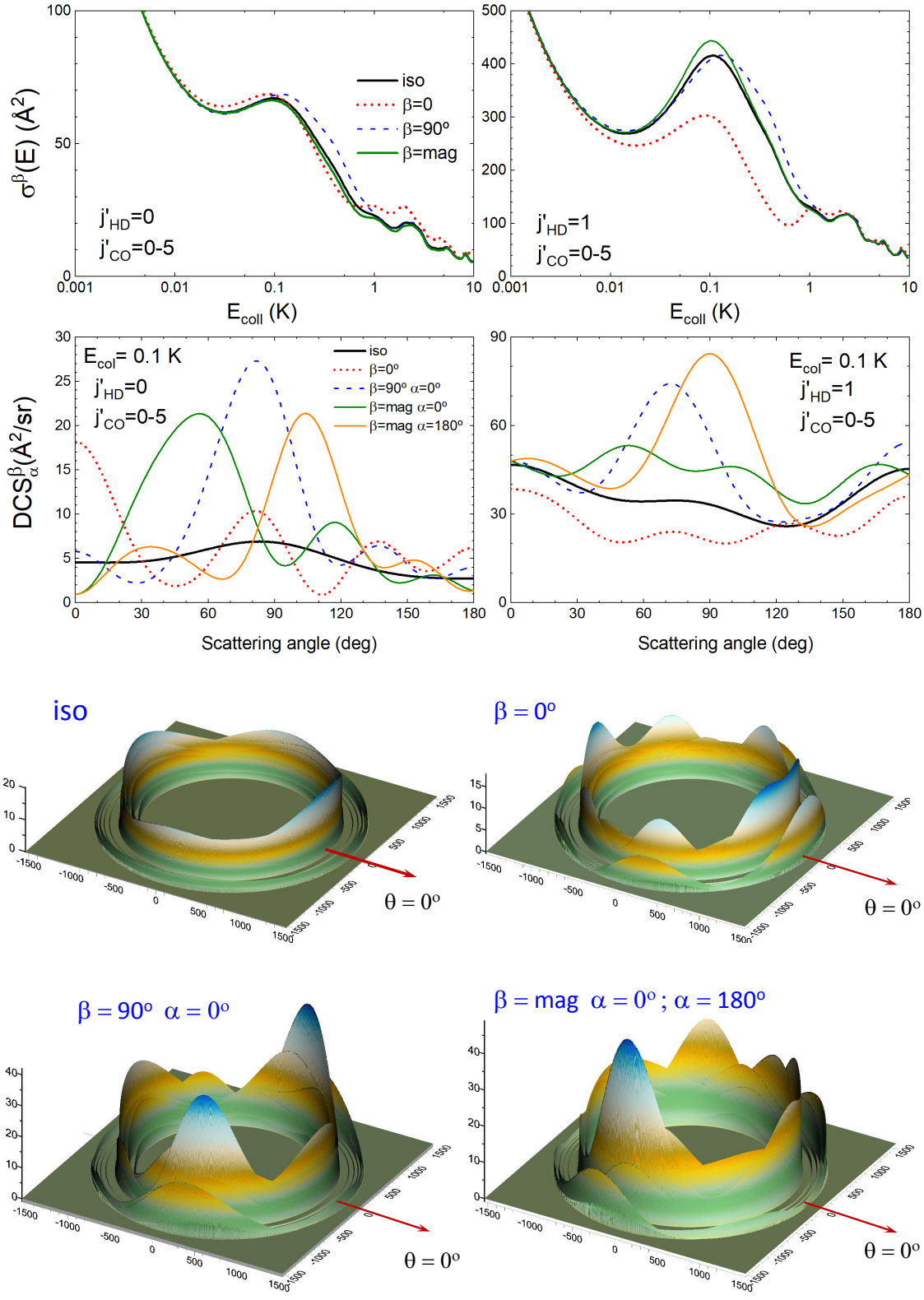

Fig. 5 Top panels: Integral cross sections as a function of the collision energy for HD(j_{HD}=2) + CO(j_{CO}=0) → HD(j'_{HD}=0,1) + CO(j'_{CO}) collisions summed over all j'_{CO} and different stereodynamical preparations. Middle panels: Differential cross sections at the peak energy of the resonance (0.1 K) for j'_{HD}=0 (left panel) and j'_{HD}=1 (right panel) summed over all j'_{CO} states. The abrupt changes in the intensity with the scattering angle for the various internuclear axis preparations are in stark contrast with the relatively featureless shape of the isotropic DCS. Four Lower panels: Scattering angle-recoil velocity polar maps at the same collision energy for the indicated internuclear axis preparations. Notice that DCS for $\beta = \text{mag}$ and α=0° differs from $\beta = \text{mag}$ and α=180°, and therefore there is no azimuthal symmetry about the incoming relative velocity. The preparation for β=90° has also no azimuthal symmetry but the DCS for α=0° and α=180° are the same.

tion function for j'_{HD}=0, and 1 (summed over all final CO rotational states). The alignment-dependent DCS are also shown in the two middle panels of 5. As can be seen, they exhibit a series of maxima that are not present in the almost featureless isotropic DCS, in particular for j'_{HD}=0. For j'_{HD}=1, the most salient features are the sideways peaks that can be observed for β=90°, α=0° and for β=mag, α=180°. These peaks can be also appreciated in the polar maps. For β=90°, α=0, 180° and β=mag, α=0,180° there is a net increase of the cross section, for both j'_{HD}. As discussed in prior studies[69], for β=mag, α=0,180° the polar map is no longer symmetrical about the relative velocity, and the two hemispheres are different. In the figure, a sideways peak is clearly appreciated for j'_{HD}=1, in the "α=180° " hemisphere, while a broader distribution is observed in the "α=0° " hemisphere. It must be stressed that the integration over the scattering angle in the (β,α)-DCSs does not correspond to the β-dependent cross sections shown in the two upper panels. Except for β=0, there is no azimuthal symmetry and, as shown in the Appendix, to reproduce the σ^{β} cross sections integration over all possible values of α (the azimuthal angle) is also required. As expected, the effect of the stereodynamical preparation on the DCSs is much more significant than on the integral cross section.

To gain more insight on how specific features of the DCS is modified by the resonance, in Fig. 6 we show the DCS calculated as a function of the collision energy and the experimental preparation for both j'_{HD}=0, and 1 (summing over all final CO rotational states). Even though the ICS at low energies is largely independent of β, the features of the DCS changes significantly with β. Moreover, for j'_{HD}=1, we observe distinct features at the energies of the resonance, which are strongly influenced by changing the relative alignment of HD angular momentum.

4 Conclusions

In this manuscript, we have studied the dynamics and stereodynamics of the inelastic collisions between HD(v=0,j=2) and CO(v=0,j=0) in the cold energy regime, i.e. for E_{coll} between 1 mK and 10 K. The main feature of the excitation functions (the energy dependence of the integral cross section) is the presence of a resonance at E_{coll}= 0.1 K, which is particularly relevant for j'_{HD}=1 final states, that are more likely to be formed than their j'_{HD}=0 counterparts.

Regardless of the final state considered, L=1 is the dominant partial-wave at the energy of the resonance peak. The relative population of L=2 at this energy depends on the final state considered, and for most of the final states the resonance is observed for both partial waves. When the L–J resolved cross sections ($\sigma^{L,J}$) are examined, we observe that many L–J combinations contribute to the resonance peak, and the relative intensity of these L–J partial waves depends on the final state considered. It is the interplay between contributions from these L–J partial waves that determines the preference towards one particular experimental preparation or another. In particular, for (j'_{HD}=1, j'_{CO}=2) higher cross section at the resonance are obtained for β=90° while β=mag is preferred for (j'_{HD}=1, j'_{CO}=1,3). In fact, the constraints imposed by the extrinsic alignment are similar to those imposed by parity conservation, making zero the cross sections for some combinations of L and J.

While at the integral cross section level, changing the polarization of j_{HD} only causes significant changes around the resonance, these changes are paramount when the DCS are analyzed, and the DCS features a series of peaks, which are appreciable in a scattering angle-recoil velocity polar map and depend on the particular preparation used.

As a whole, our results show that by tuning the polarization of one of the reactants it is possible to modify the effect of a resonance in the cold energy region for a process in which the two partners change their rotational states. Moreover, since the J-L partial waves are very dependent of the final state considered and will ultimately determine the extent of stereodynamical control, it is possible to modify to some extent the relative population of some of the product channels. While the influence of the different polarizations on the J-L partial wave is purely geometrical, the contribution from these partial waves on the isotropic cross section is solely determined by dynamics. Therefore, the overall effect of the polarization on the intensity and width of the resonance will depend on both geometrical and dynamical effects.

Appendix

The general expression for DCS for a given preparation of $\boldsymbol{j}_1$ while $\boldsymbol{j}_2$=0 or unpolarized, is[65]

$$\left[\frac{d\sigma}{d\omega}\right]^{\beta}_{\alpha} = \sum_{k=0}^{2j_1}\sum_{q=-k}^{k}(2k+1)\mathscr{A}_0^{(k)}U_q^{(k)}(\theta)C^*_{kq}(\beta,\alpha). \quad (10)$$

Inserting the expression for the PDDCS, given by Eq. (6), in Eq. (10) yields,

$$\left[\frac{d\sigma}{d\omega}\right]^{\beta}_{\alpha} = \sum_{k}\sum_{q=-k}^{k}\left(\frac{2k+1}{2j_1+1}\right)\mathscr{A}_0^{(k)}C^*_{kq}(\beta,\alpha)\sum_{m_1,\tilde{m}_1}Q_{m_1,\tilde{m}_1}\langle j_1 m_1\, kq|j_1\,\tilde{m}_1\rangle \quad (11)$$

where[70,71]

$$Q_{m_1\tilde{m}_1} = \frac{1}{2j_2+1}\sum_{m'_1m'_2}\sum_{m_2} f_{m_1,m_2\to m'_1,m'_2}\, f^*_{\tilde{m}_1,m_2\to m'_1,m'_2} \quad (12)$$

If the initial prepared state in the laboratory frame is $|j_1\,0\rangle$, where it is assumed that j is integer, then $\mathscr{A}_0^{(k)} = \langle j_1\,0\,k\,0|j_1\,0\rangle$, and

$$\left[\frac{d\sigma}{d\omega}\right]^{\beta}_{\alpha} = \sum_{m_1,\tilde{m}_1}Q_{m_1,\tilde{m}_1}\sum_{k}\sum_{q=-k}^{k}\left(\frac{2k+1}{2j_1+1}\right) \times\langle j_1\,0\,k\,0|j_1\,0\rangle\langle j_1\,m_1\,kq|j_1\,\tilde{m}_1\rangle C^*_{kq}(\beta,\alpha). \quad (13)$$

Changing the order of the C.-G. coefficients[72]:

$$\langle j_1\,0\,k\,0|j_1\,0\rangle = (-1)^{j_1}\left(\frac{2j_1+1}{2k+1}\right)^{1/2}\langle j_1\,0\;j_1\,0|k\,0\rangle \quad (14)$$

$$\langle j_1\,m_1\,k\,q|j_1\,\tilde{m}_1\rangle = (-1)^{j_1-m_1}\left(\frac{2j_1+1}{2k+1}\right)^{1/2}\langle j_1\,m_1\;j_1\;-\tilde{m}_1|k-q\rangle \quad (15)$$

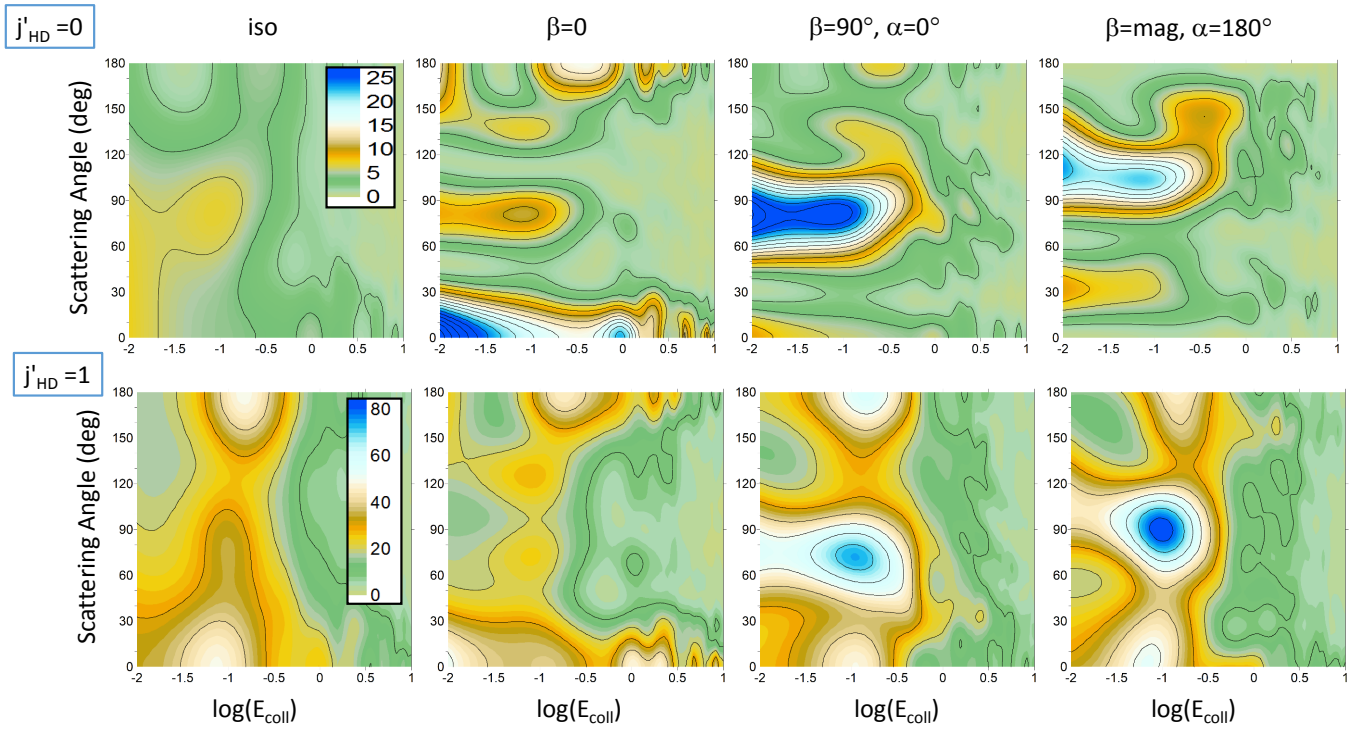

Fig. 6 Contour plots showing the collision energy dependence of the DCS for HD(j_{HD}=2) + CO(j_{CO}=0) → HD(j'_{HD})+ CO(j'_{CO}) collisions with different preparations of the HD internuclear axis. Results are summed over all j'_{CO} and are shown for j'_{HD}=0 (top panels) and j'_{HD}=1 (bottom panels).

and taking into account that

$$\left[D^k_{q0}(\alpha,\beta,0)\right]^* = C_{kq}(\beta,\alpha), \tag{16}$$

$$C^*_{kq}(\beta,\alpha) = (-1)^q C_{k-q}(\beta,\alpha) = (-1)^q \left[D^k_{-q0}(\alpha,\beta,0)\right]^*, \tag{17}$$

we obtain

$$\left[\frac{d\sigma}{d\omega}\right]^{\beta}_{\alpha} = \sum_{m_1,\tilde{m}_1} (-1)^{2j_1-m_1+q} Q_{m_1,\tilde{m}_1} \sum_k \langle j_1\, 0\; j_1\, 0|k\, 0\rangle \times \langle j_1\, m_1\; j_1\; -\tilde{m}_1|k\; -q\rangle \left[D^k_{-q0}(\alpha,\beta,0)\right]^* \tag{18}$$

where $q = \tilde{m}_1 - m_1$.

Considering the identity[72]:

$$D^{J_1}_{M'_1M_1} D^{J_2}_{M'_2M_2} = \sum_{J_3} \langle J_1M_1\, J_2M_2|J_3M_3\rangle \langle J_1M'_1\, J_2M'_2|J_3M'_3\rangle D^{J_3}_{M'_3M_3}, \tag{19}$$

if $J_1 = J_2 = j_1$, $J_3 = k$, $M_1 = M_2 = M_3 = 0$, $M'_1 = m_1$, $M'_2 = -\tilde{m}_1$ and $M'_3 = m_1 - \tilde{m}_1 = -q$

$$\left[D^{j_1}_{m_1 0}\right]^* \left[D^{j_1}_{-\tilde{m}_1 0}\right]^* = \sum_k \langle j_1\, 0\; j_1\, 0|k\, 0\rangle \langle j_1\, m_1\; j_1\; -\tilde{m}_1|k\; -q\rangle \left[D^k_{-q0}\right]^*, \tag{20}$$

or

$$(-1)^{\tilde{m}_1} C_{j_1 m_1}(\beta,\alpha) C^*_{j_1 \tilde{m}_1}(\beta,\alpha) = \sum_k \langle j_1\, 0\; j_1\, 0|k0\rangle \langle j_1\, m_1\; j_1\; -\tilde{m}_1|k\; -q\rangle \left[D^k_{-q0}\right]^*. \tag{21}$$

Substituting in Eqn. (18) and bearing in mind that $(-1)^{2j_1-2m_1+2\tilde{m}_1} = +1$ for integer j, one obtains :

$$\left[\frac{d\sigma}{d\omega}\right]^{\beta}_{\alpha} = \sum_{m_1,\tilde{m}_1} Q_{m_1\tilde{m}_1} C_{j_1m_1}(\beta,\alpha) C^*_{j_1\tilde{m}_1}(\beta,\alpha) = \frac{1}{2j_2+1} \sum_{m'_1m'_2} \sum_{m_2} \left| \sum_{m_1} C_{j_1m_1}(\beta,\alpha) f_{m_1,m_2\to m'_1,m'_2} \right|^2. \tag{22}$$

In those cases in which the experiment is carried out under conditions that imply azimuthal symmetry, Eq. (22) ought to be integrated over the azimuthal angle α if the ***k*-*k***′ plane is taken as the reference or over $\phi - \alpha$ if a different reference plane is chosen. The resulting expression is

$$\int_0^{2\pi} d\alpha \left[\frac{d\sigma}{d\omega}\right]^{\beta}_{\alpha} = \sum_{m_1,\tilde{m}_1} 2\pi\delta_{m_1,\tilde{m}_1}\; Q_{m_1\tilde{m}_1} C_{j_1m_1}(\beta,0) C_{j_1,\tilde{m}_1}(\beta,0) = 2\pi \sum_{m_1} Q_{m_1,m_1} \left[C_{jm_1}(\beta,0)\right]^2. \tag{23}$$

Additional integration over $\cos\theta$ leads to the 'directional' integral

cross section for one of reagents prepared with internuclear axis along β:

$$\sigma^{\beta} = \int_{-1}^{1}\int_{0}^{2\pi} \mathrm{d}(\cos\theta)\,\mathrm{d}\alpha \left[\frac{\mathrm{d}\sigma}{\mathrm{d}\omega}\right]_{\alpha}^{\beta} = \sum_{m_1} \sigma_{m_1} \left[C_{j_1 m_1}(\beta,0)\right]^2 \quad (24)$$

where σ_{m_1} is the integral cross section for the m_1 state, averaged over m_2 and summed over m_1' and m_2'

$$\sigma_{m_1} = \frac{1}{2j_2+1} \sum_{m_1',m_2'} \sum_{m_2} \sigma_{m_1 m_2 \to m_1' m_2'}. \quad (25)$$

It should be stressed that Eqns. (22)–(24) are only valid as long as the prepared state is $|j_1\,0\rangle$.

Conflicts of interest

There are no conflicts to declare.

Acknowledgements

PGJ and FJA thank Prof. Enrique Verdasco and Jesús Aldegunde for their support and help with the calculations. Funding by the Spanish Ministry of Science and Innovation (grant PGC2018-096444-B-I00, and PID2020-113147GA-I00) is acknowledged. P.G.J. acknowledges funding by Fundación Salamanca City of Culture and Knowledge (programme for attracting scientific talent to Salamanca). N.B. acknowledges support from NSF [Grant No. PHY-1806334] and ARO MURI [Grant No. W911NF-19-1-0283].

Notes and references

1 L. D. Carr, D. DeMille, R. V. Krems and J. Ye, *New J. Phys.*, 2009, **11**, 055049.
2 R. V. Krems, *Molecules in Electromagnetic Fields*, John Wiley & Sons, Ltd, 2018.
3 N. Balakrishnan, *J. Chem. Phys.*, 2016, **145**, 150901.
4 J. L. Bohn, A. M. Rey and J. Ye, *Science*, 2017, **357**, 1002–1010.
5 J. Toscano, H. J. Lewandowski and B. R. Heazlewood, *Phys. Chem. Chem. Phys.*, 2020, **22**, 9180–9194.
6 M.-G. Hu, Y. Liu, D. D. Grimes, Y.-W. Lin, A. H. Gheorghe, R. Vexiau, N. Bouloufa-Maafa, O. Dulieu, T. Rosenband and K.-K. Ni, *Science*, 2019, **366**, 1111–1115.
7 Y. Liu, M.-G. Hu, M. A. Nichols, D. D. Grimes, T. Karman, H. Guo and K.-K. Ni, *Nat. Phys.*, 2020, 1132–1136.
8 Y. Segev, M. Pitzer, M. Karpov, N. Akerman, J. Narevicius and E. Narevicius, *Nature*, 2019, **572**, 189–193.
9 M.-G. Hu, Y. Liu, M. A. Nichols, L. Zhu, G. Quéméner, O. Dulieu and K.-K. Ni, *Nat. Chem.*, 2021, **13**, 435–440.
10 H. Son, J. J. Park, W. Ketterle and A. O. Jamison, *Nature*, 2020, **580**, 197–200.
11 B. K. Kendrick, H. Li, M. Li, S. Kotochigova, J. F. E. Croft and N. Balakrishnan, *Phys. Chem. Chem. Phys.*, 2021, **23**, 5096–5112.
12 M. Weyland, S. S. Szigeti, R. A. B. Hobbs, P. Ruksasakchai, L. Sanchez and M. F. Andersen, *Phys. Rev. Lett.*, 2021, **126**, 083401.
13 W. B. Cairncross, J. T. Zhang, L. R. B. Picard, Y. Yu, K. Wang and K.-K. Ni, *Phys. Rev. Lett.*, 2021, **126**, 123402.
14 V. V. Albert, J. P. Covey and J. Preskill, *Phys. Rev. X*, 2020, **10**, 031050.
15 Y. Wan, B. H. Yang, P. C. Stancil, N. Balakrishnan, N. J. Parekh and R. C. Forrey, *The Astrophysical Journal*, 2018, **862**, 132.
16 Y. Wan, N. Balakrishnan, B. H. Yang, R. C. Forrey and P. C. Stancil, *Monthly Notices of the Royal Astronomical Society*, 2019, **488**, 381–386.
17 A. G. G. M. Tielens, *Rev. Mod. Phys.*, 2013, **85**, 1021–1081.
18 W. E. Perreault, N. Mukherjee and R. N. Zare, *Science*, 2017, **358**, 356–359.
19 W. E. Perreault, N. Mukherjee and R. N. Zare, *Nat. Chem.*, 2018, **10**, 561–567.
20 W. E. Perreault, N. Mukherjee and R. N. Zare, *J. Chem. Phys.*, 2019, **150**, 174301.
21 W. E. Perreault, N. Mukherjee and R. N. Zare, *J. Chem. Phys.*, 2020, **152**, 209901.
22 H. Zhou, W. E. Perreault, N. Mukherjee and R. N. Zare, *J. Chem. Phys.*, 2021, **154**, 104309.
23 J. F. E. Croft, N. Balakrishnan, M. Huang and H. Guo, *Phys. Rev. Lett.*, 2018, **121**, 113401.
24 J. F. E. Croft and N. Balakrishnan, *J. Chem. Phys.*, 2019, **150**, 164302.
25 P. G. Jambrina, J. F. E. Croft, H. Guo, M. Brouard, N. Balakrishnan and F. J. Aoiz, *Phys. Rev. Lett.*, 2019, **123**, 043401.
26 M. Lara, P. G. Jambrina, F. J. Aoiz and J. M. Launay, *J. Chem. Phys.*, 2015, **143**, 204305.
27 M. Lara, P. G. Jambrina, J. M. Launay and F. J. Aoiz, *Phys. Rev. A*, 2015, **91**, 030701.
28 P. G. Jambrina, L. González-Sánchez, M. Lara, M. Menéndez and F. J. Aoiz, *Phys. Chem. Chem. Phys.*, 2020, **22**, 24943.
29 M. Morita and N. Balakrishnan, *J. Chem. Phys.*, 2020, **153**, 184307.
30 T. V. Tscherbul and J. Kłos, *Phys. Rev. Research*, 2020, **2**, 013117.
31 A. Devolder, T. Tscherbul and P. Brumer, *Phys. Rev. A*, 2020, **102**, 031303.
32 A. Devolder, P. Brumer and T. V. Tscherbul, *Phys. Rev. Lett.*, 2021, **126**, 153403.
33 C. Amarasinghe and A. G. Suits, *J. Phys. Chem. Lett.*, 2017, **8**, 5153–5159.
34 C. Amarasinghe, C. A. Perera and A. G. Suits, *J. Chem. Phys.*, 2020, **152**, 184201.
35 A. B. Henson, S. Gersten, Y. Shagam, J. Narevicius and E. Narevicius, *Science*, 2012, **338**, 234–238.
36 Y. Shagam, A. Klein, W. Skomorowski, R. Yun, V. Averbukh, C. P. Koch and E. Narevicius, *Nat. Chem.*, 2015, **7**, 921–926.
37 A. Klein, Y. Shagam, W. Skomorowski, P. S. Żuchowski, M. Pawlak, L. M. C. Janssen, N. Moiseyev, S. Y. T. van de Meerakker, A. van der Avoird, C. P. Koch and E. Narevicius, *Nat. Phys.*, 2017, **13**, 35–38.
38 P. G. Jambrina, M. Menéndez, A. Zanchet, E. García and F. J. Aoiz, *Phys. Chem. Chem. Phys.*, 2019, **21**, 14012–14022.

39 P. G. Jambrina, J. Aldegunde, F. J. Aoiz, M. Sneha and R. N. Zare, *Chem. Sci.*, 2016, **7**, 642.

40 M. Morita, Q. Yao, C. Xie, H. Guo and N. Balakrishnan, *Phys. Rev. Research*, 2020, **2**, 032018.

41 P. Jankowski and K. Szalewicz, *J. Chem. Phys.*, 1998, **108**, 3554–3565.

42 A. V. Potapov, L. A. Surin, V. A. Panfilov, B. S. Dumesh, T. F. Giesen, S. Schlemmer, P. L. Raston and W. Jäger, *Astrophys. J*, 2009, **703**, 2108–2112.

43 B. Yang, P. C. Stancil, N. Balakrishnan and R. C. Forrey, *Astrophys. J*, 2010, **718**, 1062–1069.

44 P. Jankowski, A. R. W. McKellar and K. Szalewicz, *Science*, 2012, **336**, 1147–1150.

45 P. Jankowski, L. A. Surin, A. Potapov, S. Schlemmer, A. R. W. McKellar and K. Szalewicz, *J. Chem. Phys.*, 2013, **138**, 084307.

46 S. Chefdeville, T. Stoecklin, A. Bergeat, K. M. Hickson, C. Naulin and M. Costes, *Phys. Rev. Lett.*, 2012, **109**, 023201.

47 B. Yang, P. Zhang, X. Wang, P. C. Stancil, J. M. Bowman, N. Balakrishnan and R. C. Forrey, *Nat. Comm.*, 2015, **6**, 6629.

48 S. Chefdeville, T. Stoecklin, C. Naulin, P. Jankowski, K. Szalewicz, A. Faure, M. Costes and A. Bergeat, *Astrophys. J*, 2015, **799**, L9.

49 R. C. Forrey, B. Yang, P. Stancil and N. Balakrishnan, *Chem. Phys.*, 2015, **462**, 71–78.

50 M. Costes and C. Naulin, *Chem. Sci.*, 2016, **7**, 2462–2469.

51 A. Faure, P. Jankowski, T. Stoecklin and K. Szalewicz, *Scientific Reports*, 2016, **6**, 28449.

52 A. Andrews and C. Simpson, *Chem. Phys. Lett.*, 1976, **41**, 565–569.

53 W. S. Drozdoski, R. M. Young, R. D. Bates and J. K. Hancock, *J. Chem. Phys.*, 1976, **65**, 1542–1549.

54 M. Turnidge, G. Wilson and C. Simpson, *Chem. Phys. Lett.*, 1994, **227**, 45–50.

55 R. Krems, TwoBC – quantum scattering program, University of British Columbia, Vancouver, Canada, 2006.

56 A. M. Arthurs and A. Dalgarno, *Proc. Roy. Soc. London, Ser. A*, 1960, **256**, 540–551.

57 G. Quéméner, N. Balakrishnan and R. V. Krems, *Phys. Rev. A*, 2008, **77**, 030704.

58 G. Quéméner and N. Balakrishnan, *J. Chem. Phys.*, 2009, **130**, 114303.

59 S. F. dos Santos, N. Balakrishnan, S. Lepp, G. Quéméner, R. C. Forrey, R. J. Hinde and P. C. Stancil, *J. Chem. Phys.*, 2011, **134**, 214303.

60 A. Faure, P. Jankowski, T. Stoecklin and K. Szalewicz, *Sci. Rep.*, 2016, **6**, 28449.

61 G. Garberoglio, P. Jankowski, K. Szalewicz and A. H. Harvey, *J. Chem. Phys.*, 2017, **146**, 054304.

62 N. Balakrishnan, J. F. E. Croft, B. H. Yang, R. C. Forrey and P. C. Stancil, *Astrophys. J*, 2018, **866**, 95.

63 D. E. Manolopoulos, *J. Chem. Phys.*, 1986, **85**, 6425–6429.

64 J. Schaefer and W. Meyer, *J. Chem. Phys.*, 1979, **70**, 344.

65 J. Aldegunde, M. P. de Miranda, J. Haigh, B. K. Kendrick, V. Sáez-Rábanos and F. J. Aoiz, *J. Phys. Chem. A*, 2005, **109**, 6200.

66 S. Kais and R. D. Levine, *J. Phys. Chem.*, 1987, **91**, 5462–5465.

67 K. Blum, *Density Matrix Theory and Applications*, Plenum, New York, 1986.

68 J. Aldegunde, J. M. Alvariño, M. P. de Miranda, V. Sáez Rábanos and F. J. Aoiz, *J. Chem. Phys*, 2006, **125**, 133104.

69 F. Wang, J.-S. Lin and K. Liu, *J. Chem. Phys.*, 2014, **140**, 084202.

70 C. G. Heid, V. Walpole, M. Brouard, P. G. Jambrina and F. J. Aoiz, *Nat. Chem.*, 2019, **11**, 662.

71 V. Walpole, C. G. Heid, P. G. Jambrina, F. J. Aoiz and M. Brouard, *J. Phys. Chem. A*, 2019, **123**, 8787.

72 R. N. Zare, *Angular Momentum*, Wiley, 1988.